# Experimental results from field tests on a 225 kV HVAC cable

I. Lafaia, J. Mahseredjian, A. Ametani, M. T. Correia de Barros, I. Koçar, Y. Fillion.

***Abstract*-- This paper presents experimental results from two field tests carried out on a 225 kV underground XLPE cable with 64 km and 17 major sections with cross-bonding of sheaths. The first test applied a 2 kV surge to a minor and a major sections having 1080 m and 3952 m, respectively. The second field test measured the transient current and voltage when energizing the full cable. Measured results of current show the impact of transformers in the network and the reactive compensator. The energization test is simulated in EMTP using detailed and simplified cable models. Using the simplified model does not reduce the accuracy of simulations of core voltages and currents.**

***Keywords*: underground cable, field tests, electromagnetic transients, EMTP.**

## I. Introduction

PROJECTS of new cable installations have taken place worldwide in the last few years. These cable links are used for intercontinental connections, to reinforce the grid with reduced impact in the surrounding environment, and to connect to renewable energy sources to the grid [1]-[5].

The increase of computer capacity and the improvement of simulation tools allowed the development of more accurate cable models used for electromagnetic transient (EMT) studies, cable fault location and harmonic studies [6]-[13]. A cable model can be validated based on simulations only [6]-[11], but a more reliable validation requires a comparison of the simulation results with measurements from field tests performed on the actual cable system [7],[9],[13]-[18].

This paper presents experimental results from two field tests carried out on a high-voltage alternate-current (HVAC) cable. The first field test applied a 2 kV surge to a minor and a major sections of the cable having 1080 m and 3952 m, respectively. The advantage of testing a single minor section is that we can excite each propagation mode separately and observe the respective cable responses, which is useful for model validation. The second field test measured the transient current and voltage when connecting the full cable to the grid. The energization test is simulated in EMTP.

I. Lafaia, A. Ametani, J. Mahseredjian, and I. Kocar are with Polytechnique Montreal, 2500 Chemin de Polytechnique, Montréal (Québec) H3T1J4, Canada (e-mail: isabel.lafaia.ca@ieee.org

M. T. Correia de Barros is with Instituto Superior Técnico, University of Lisbon, Avenida Rovisco Pais 1, 1049-001 Lisboa, Portugal.

Y. Fillion is with Réseaux de Transport d'Électricité, Cœur Defénce-100 esplanade du Général de Gaulle, 92932 Paris La Défense Codex, France.

Paper submitted to the International Conference on Power Systems Transients (IPST2017) in Seoul, Republic of Korea June 26-29, 2017

## II. Cable system

The tested system is a 225 kV XLPE underground cross-bonded cable with 64 km length. The cable phases are enclosed by high-density poly-ethylene (HDPE) tubes embedded in concrete. Fig. 1 shows the layout of the cable and Table 1 contains the cable data. The cable has 17 major sections. The cross-bonding joints of the terminal major sections are protected by surge arresters. Reactive compensators are connected at both cable ends.

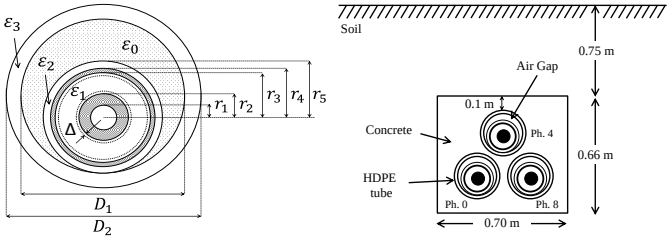


Fig. 1. Layout of the 225 kV XLPE underground cable: a) one-phase layout; b) burial layout.

TABLE 1. DATA FOR 225 KV XLPE UNDERGROUND CABLE

| Parameter | 2000 mm$^2$ cable | 2500 mm$^2$ cable |
|---|---|---|
| Core cond. ($r_1 = 0$), $\rho = 1.76\times10^{-8}$ Ωm | $r_{2n} = 34.5$ mm* <br> $r_2 = 28.4$ mm** | $r_{2n} = 37.1$ mm* <br> $r_2 = 31.9$ mm** |
| Semicond. screens | $\Delta = 3$ mm (thickness) | |
| Core insulation | $\varepsilon_{r1} = 2.5$, $\tan\delta = 0.0008$ | |
| Metallic sheath $\rho = 2.84\times10^{-8}$ Ωm | $r_3 = 56.4$ mm, <br> $r_4 = 57.2$ mm | $r_3 = 59.9$ mm, <br> $r_4 = 60.7$ mm |
| Outer insulation $\varepsilon_{r2} = 2.5$ $\tan\delta = 0.001$ | $r_5 = 62.2$ mm | $r_5 = 65.7$ mm |
| HDPE tubes | $D_1 = 198.5$ mm, $D_2 = 225$ mm <br> $\varepsilon_{r3} = 2.5$, $\tan\delta = 0.001$ | |

* Nominal radius of core conductor.

** Corrected radius accounting for section of wires in the strand.

## III. Surge test

This test applied a 2 kV 1.2/50 μs surge to a minor and a major cable sections having 1080 m and 3952 m, respectively. The generator output impedance is 2 Ω. Grounding rods had to be installed next to the two terminals of the minor section and the receiving end of the major section, for protection of equipment and operators. The major section sending end is located in a substation where a grounding network is available. The DC values of grounding resistance are 30 Ω (measured) for the remote areas and 5 Ω (provided by RTE) for the substation.

### A. Minor section, surge application to core

The circuits in Fig. 2 were used in the field test to apply an impulse to the core of a minor section and measure the sheath voltage of the same phase. The two circuits are for the case of all sheaths open-circuited and for the case of sheaths grounded (except the measured sheath).

Fig. 3 shows the measured sheath voltages. The high waveform attenuation indicates that the mode observed is an earth-return mode. There is also a contribution of a coaxial mode which can be observed from the peaks in the waveforms in Fig. 3. Using the cable length and the time between the second and third peaks (12.6 μs), the propagation speed is calculated as $2\times1080/12.6=171\,\mathrm{m/\mu s}$ which is close to the value calculated from the light speed $c_0=300\,\mathrm{m/\mu s}$ and the cable insulation permittivity $\varepsilon_r=3.23$ (section V.A.2) as $c=c_0/\sqrt{\varepsilon_r}=300/\sqrt{3.23}=167\,\mathrm{m/\mu s}$.

In Fig. 3, the voltage corresponding to the sheaths being grounded becomes negative after a certain time as a result of negative reflections transmitted from grounded terminals.

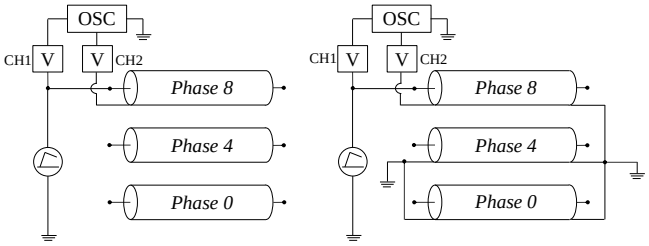


Fig. 2. Field test circuits for core-to-ground surge application on a minor section: a) sheaths open; b) sheaths grounded.

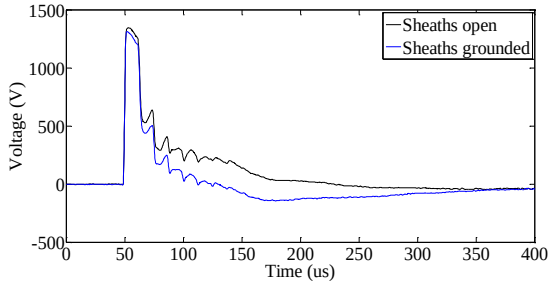


Fig. 3. Sending end sheath voltage for core-to-ground surge application on a minor section.

Fig. 4 illustrates the circuit used in the field test to apply a surge between the core and sheath of a phase in a minor section. The three sheaths and the two non-used cores were grounded together with the surge tester. The core voltage at the sending end is shown in Fig. 5. The spikes observed are caused by the inductance of the wire connecting to the tester and the fast variation of current.

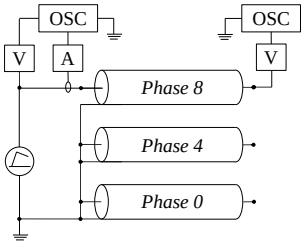


Fig. 4. Test circuit for core-to-sheath surge application on a minor section.

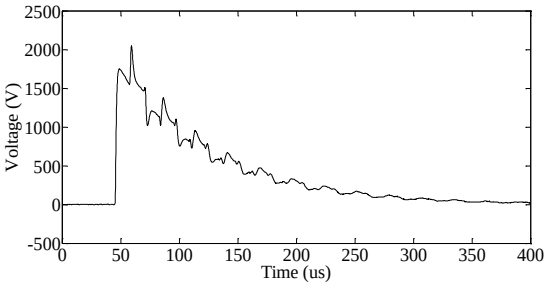


Fig. 5. Sending end core voltage for core-to-sheath surge application on a minor section.

### B. Minor section, inter-sheath surge application

The circuit in Fig. 6a was used in the field test to apply a surge between two sheaths of a minor section. The sheath voltage at the sending ends is shown in Fig. 7. Using the average time between same-polarity peaks (42.1 μs) and the length of the minor section, the propagation speed is calculated as $v=4\times1080/42.1=102.6\ \mathrm{m/\mu s}$. The initial sheath voltage in Fig. 7 is substantially lower that the applied surge of 2 kV, which shows that the source grounding has an important effect on the measured result.

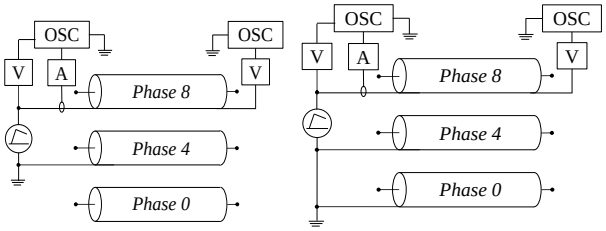


Fig. 6. Surge test circuit for inter-sheath surge application on a minor section: a) two-phase application; b) three-phase application.

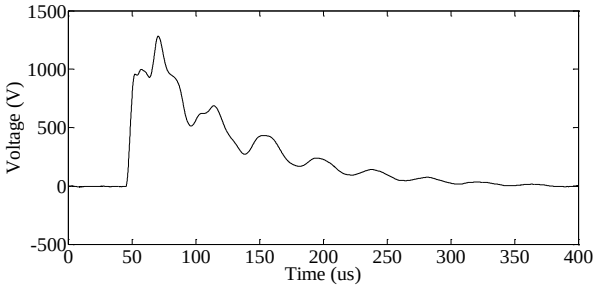


Fig. 7. Sending end voltage for 2-phase inter-sheath surge application on a minor section.

The circuit in Fig. 6b was used in the field test to apply a surge between the sheaths of the minor section, involving all the three phases. The waveforms measured at sending and receiving ends are shown in Fig. 8 and Fig. 9. The period of oscillations of voltage waveforms at the receiving end is approximately 38 μs. Using the cable length, the propagation speed is calculated as $c=4\times1080/38=114\,\mathrm{m/\mu s}$. This result shows that the 2-phase and 3-phase inter-sheath modes have different speeds: 114 m/μs compared to 102.6 m/μs calculated from Fig. 7. The speed of the 3-phase inter-sheath mode is higher because the current returns through 2 phases instead of 1. Therefore, the inductance of the current path is lower (parallel of the 2 phases) and the speed is higher.

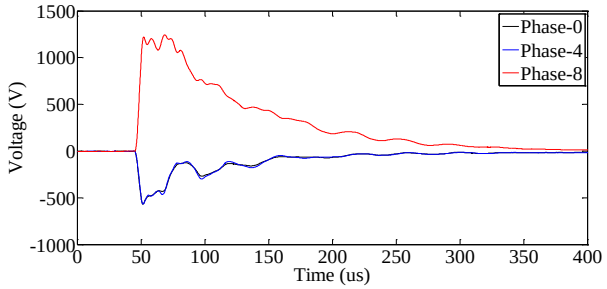


Fig. 8. Sending end voltages for 3-phase inter-sheath surge application on a minor section.

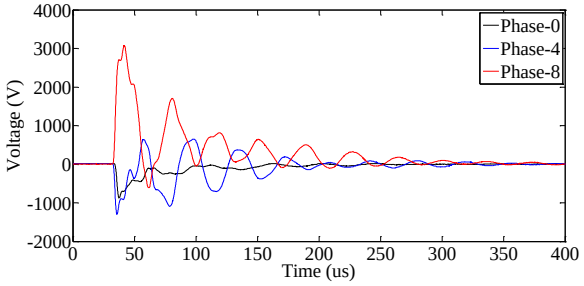


Fig. 9. Receiving end voltages for 3-phase inter-sheath surge application on a minor section.

### C. Minor section, sheath-to-ground application

The circuit of Fig. 10 was used in the field test to apply a surge between the sheaths and the ground, with the receiving end open-circuited. The sheath voltages measured at the receiving end of the minor section are shown in Fig. 11 to Fig. 13 with peak values of 1149 V, 750 V and 623 V for surge applied to one sheath, two sheaths, and three sheaths, respectively. The differences in peak voltages are due to the current splitting between one, two and three sheaths. The ratio between the voltages is not simply 1/3 and 1/2 as could be expected because the current returns through the ground and thus the earth-return impedance has a major impact in the result.

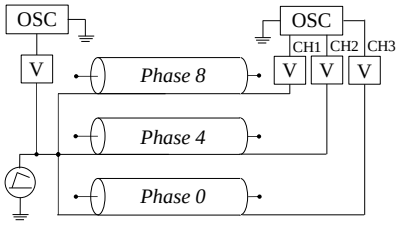


Fig. 10. Surge test circuit for earth-return mode excitation on a minor section.

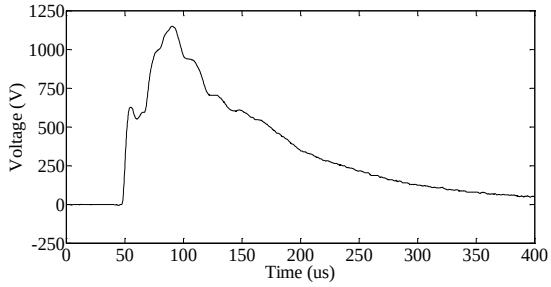


Fig. 11. Receiving end voltage for surge application on one sheath of a minor section with the receiving end in open-circuit.

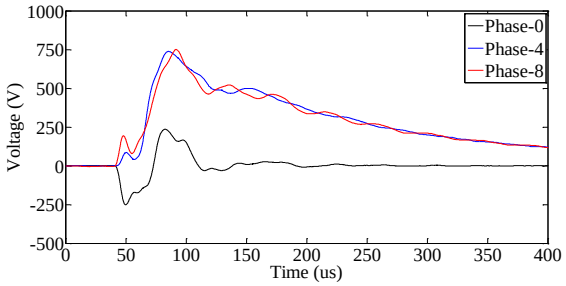


Fig. 12. Receiving end voltages for surge application on two sheaths of a minor section with the receiving end in open-circuit.

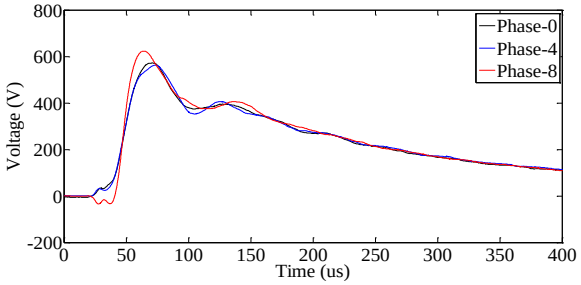


Fig. 13. Receiving end voltages for surge application on three sheaths of a minor section with the receiving end in open-circuit.

### D. Major section, sheath-to-ground application

The circuit in Fig. 14 was used in the field test to measure the response of a major section to a surge applied between the three sheaths and the ground. The test was repeated with the sheaths at the receiving end open-circuited, bonded, and grounded, respectively. The sending end sheath voltage and the source current are shown in Fig. 15 and Fig. 16.

Both results with open-ended sheaths and short-circuited sheaths in Fig. 15, show a positive reflection at 225 μs. Using that value and the cable length, the propagation speed is calculated as $v = 4 \times 3953/225 = 70\,\mathrm{m/\mu s}$ . This positive voltage reflection is accompanied by a negative current reflection observed in Fig. 16. The reflections are not observed in the case of sheath grounded at the receiving end because in this case the earth-return loop is not interrupted.

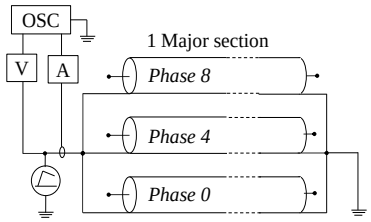


Fig. 14. Surge test circuit for sheath to ground application on a major section.

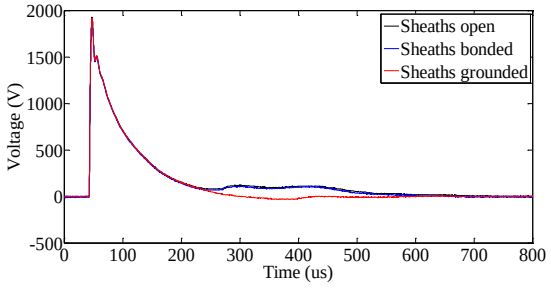


Fig. 15. Sending end sheath voltages for zero-sequence surge application to the sheaths of a major section for different sheath terminations.

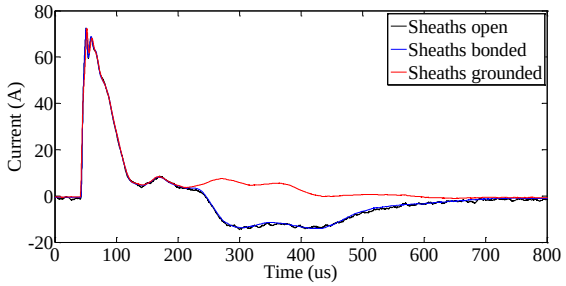


Fig. 16. Sending end currents for zero-sequence surge application to the sheaths of a major section for different sheath terminations.

## IV. Energization Test

An energization test of the full RTE 225 kV cable was carried out before the cable was put in service. The sending end is in the substation of Boutre with a short-circuit power of 7740 MVA at the time of the test and the receiving end is in the substation of Trans (Trans-en-Province) with 4194 MVA. Both substations have X/R ≈ 7. A shunt compensator of 80 Mvar and 175 kW at 225 kV is located at the Trans terminal. The cable was first energized from the substation of Boutre, with the far end open-circuited. The cable was then energized from the substation of Trans. This is illustrated in Fig. 17.

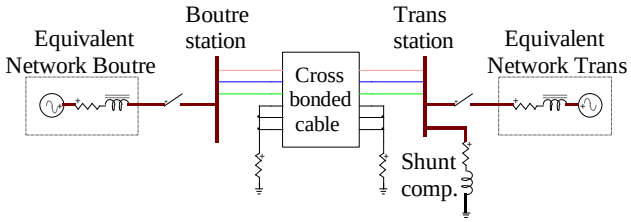


Fig. 17. Field test circuit for energising the RTE 225 kV cable.

### A. Energization from Boutre substation

Fig. 18 shows the currents and voltages measured when the cable was energised at the Boutre substation. The closing times are t = 4.5 ms, t = 6 ms and t = 6 ms for phase-0, phase-4 and phase-8, respectively. Fig. 19 shows the details of the transient current. The initial current drawn by the cable is very high. Phase-8 has an initial peak of 3533 A which damps out to 776 A after 5 cycles (100 ms). The peak currents in the other phases are 3210 A in phase-0 and 3151 A in phase-4. The voltage reaches steady-state faster than the current, which does not attain steady-state during the measurement. This is caused by resonance due to transformers in the network.

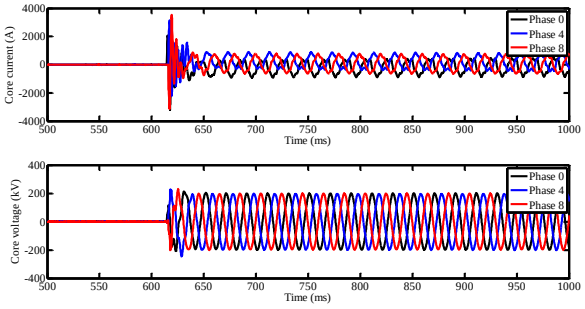


Fig. 18. Currents and voltages during energization of the cable from the substation of Boutre.

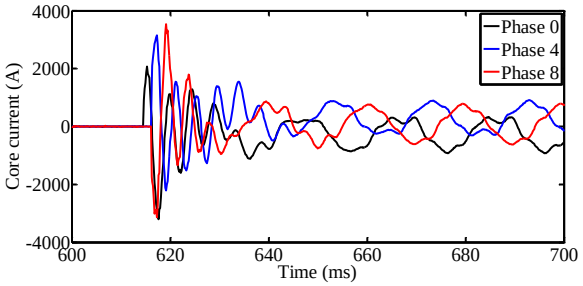


Fig. 19. Initial transient currents during energization of the cable from the substation of Boutre.

### B. Energization from Trans substation

Fig. 20 shows the currents and voltages measured during the energization of the cable from the Trans substation. The source is applied at t = 648.3 ms for phase-0, t = 646.7 ms for phase-4 and t = 648ms for phase-8. The detailed current waveforms are shown in Fig. 21. The currents have a decaying DC component due to the shunt compensator. After energization, the voltages are reduced from 1.09 pu to 1.04 pu which shows that the network absorbed part of the reactive power generated by the cable.

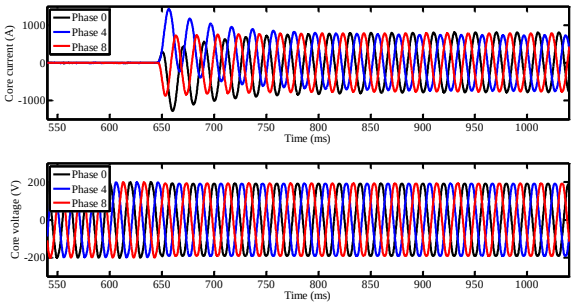


Fig. 20. Currents and voltages during energization of the cable from the substation of Trans.

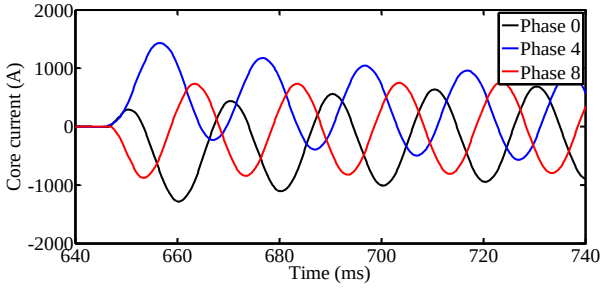


Fig. 21. Initial transient currents during energization of the cable from the substation of Trans.

## V. Simulation of Cable Energization in EMTP

### A. Cable modeling

The 225 kV cable is modeled in EMTP using a wideband phase-domain model [19]-[21]. Classical cable data calculation functions in EMT-type software (e.g. [22],[23]) cannot handle features such as semiconducting screens, stranded core conductors and HDPE tubes. These require corrections to the input data as explained next [25].

*1) Core and Metallic Sheath Conductors*

The sheath conductor is modeled as a hollow cylindrical

conductor with the resistivity given in Table 1. Eddy currents caused by proximity between sheaths are neglected due to the wide separation between the phases. The core conductor, made of stranded enameled copper $\left(\rho_{copper} = 1.76\times10^{-8}\,\Omega\text{m}\right)$, requires a modification of the resistivity to account for the gaps between the strand wires which reduce the effective section of the core conductor. The modified resistivities become $2.6\times10^{-8}\,\Omega\text{m}$ and $2.83\times10^{-8}\,\Omega\text{m}$ for the 2000 mm$^2$ and 2500 mm$^2$ core cables, respectively [24],[25].

*2) Core Insulation and Semiconducting Screens*

The cable semiconducting (SC) layers may have an important impact on the propagation of coaxial waves, particularly affecting the shunt admittance [26]. To account for SC layers, it is generally accurate enough to use a modified value of permittivity to account for the new thickness of the cable insulation [25],[26]. The modified values of $\varepsilon'_{r1}$ become 3.23 and 3.22 for the 2000 mm$^2$ and 2500 mm$^2$, respectively [25].

*3) Outer Insulation and HDPE Tube*

The outer cable insulation is composed of three layers, i.e. the sheath insulation, the air gap, and the HDPE tube (see Fig. 1), which are not concentric (the cable lies on the bottom of the tube). The impact of the HDPE tubes can be modeled by a modified permittivity of the sheath insulation calculated as explained in [27]. The modified permittivities become $\varepsilon_{r2_{eq}} = 0.339$ and 0.371 for 2000 mm$^2$ and 2500 mm$^2$ cables.

*4) Cross-bonding points and sheath grounding*

The cross-bonding of the 225 kV cable uses 300 mm² copper wires with an inductance of 20 μH connecting the metallic sheaths of adjacent minor sections [16]. The sheath grounding impedance is also modeled by 5 Ω.

### *B. Modeling of energising circuits*

The networks at the two cable ends are modeled by balanced voltage sources in series with coupled *RL* branches. The shunt compensator at the Trans substation is modeled by an uncoupled three-phase *RL* branch. The values of the *RL* branches are derived from the short-circuit power and R/X ratio given in section IV.

### *C. Simulation results*

Two alternative cable models are used to simulate the energization test presented in section IV. Model 1 uses a separate model for each cable minor section. Model 2 uses a homogeneous equivalent for the whole cable length, assuming all cable sections having 2000 mm$^2$ core conductors.

Fig. 22 shows the field test results of current and voltage at the cable sending end for energising from the Boutre substation as well as the simulated results. Cable models 1 and 2 show nearly the same response. This is because the reflections transmitted from cross-bonding points are highly attenuated by the network.

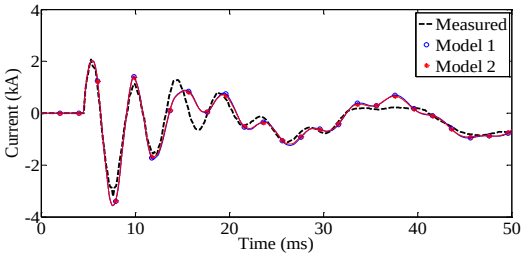


a) Phase-0 sending end current.

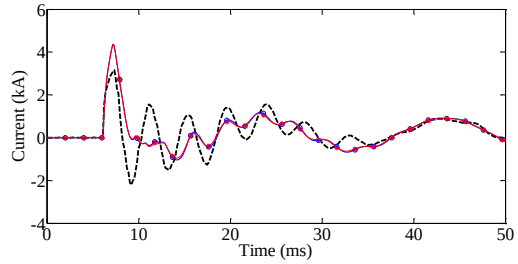


b) Phase-4 sending end current.

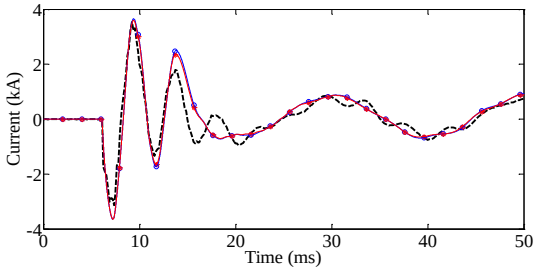


c) Phase-8 sending end current.

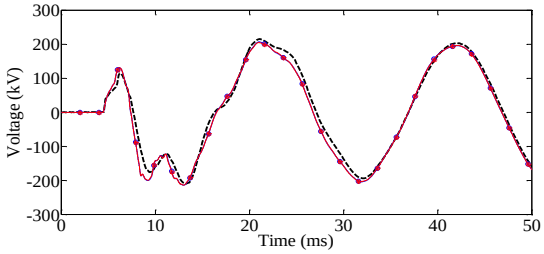


d) Phase-0 sending end voltage.

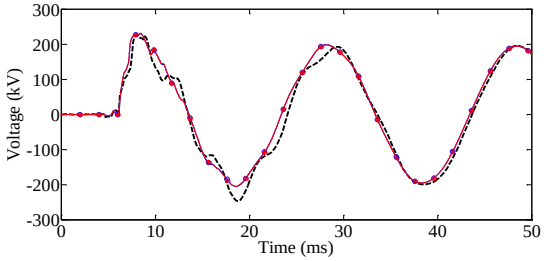


e) Phase-4 sending end voltage.

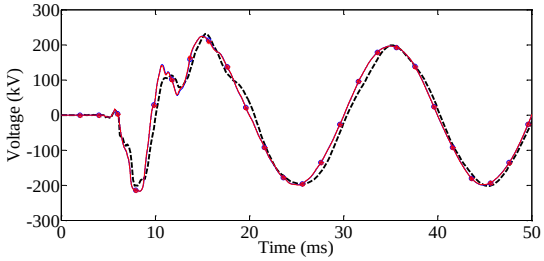


f) Phase-8 sending end voltage.

Fig. 22. Field test and simulation results, energization of the cable from the Boutre substation.

### D. Discussion

Several conclusions are drawn from the results in Fig. 22. Firstly, detailed modeling of every minor section of the cable (model 1 in Fig. 22) does not improve the agreement with measured results when compared to model 2, which uses one single wide-band segment to represent the whole cable, even though model 1 requires a significantly larger effort for circuit setup and computation.

Secondly, the fact that the two cable models in Fig. 22 generate the same results shows that the transient involves mainly inter-core modes. In that case, accurate modeling of the core and sheath conductors, as well as semiconducting layers, explained in section V.A is important as these have direct impact on the characteristics of core modes. On the other hand, accurate modeling of HDPE tubes and cross-bonding wires have little impact on the results of Fig. 22.

The above conclusions are valid because the simulated test concerned only core conductor quantities. If sheath voltages and currents had to be simulated, then model 2 might not be accurate enough.

Another important aspect in the simulation of the energization test is the modeling of the equivalent networks. As observed in section IV, the core currents are particularly affected by the network having a longer transient than the measured voltages. This is due to the effect of transformers in the network. Therefore, a more accurate modeling of the equivalent networks could possibly improve the simulation results for the currents in Fig. 22.

## VI. Conclusions

This paper presented a surge test and an energization test carried out on a 225 kV underground AC cable. The energization test was simulated in EMTP using two alternative cable models and it was found that using a single wideband segment to model the whole cable length does not reduce the accuracy of simulations as far as core voltages and currents are concerned. The simulation results of currents are less accurate than the results of voltages due to the modeling of the equivalent network which does not represent the impact of transformers inside that network.

## VII. References


[1] CIGRE WG C4.502, "power system technical performance issues related to the application of long HVAC cables", CIGRE TB 556, Oct. 2013.

[2] L. Colla, M. Robolini, and F. Iliceto, "400 kV AC new submarine cable links new between Sicily and the Italian mainland", CIGRE 2008 General Session, paper C4-116, Paris, Aug. 2008.

[3] Energinet.dk, "Cable Action Plan", www.energinet.dk, March 2009.

[4] S. Lauria and F. Paolone, "Optimal operation of long inhomogeneous AC cable lines: the Malta–Sicily interconnector", IEEE TPWD, vol. 29, pp. 1036-1044, 2014.

[5] Réseaux de Transport d'Électricité, "Filet de sécurité PACA: pour une sécurisation électrique durable de la région", http://www.rte-france.com/fr/projet/filet-de-securite-paca-pour-une-securisation-electrique-durable-de-la-region (May 2015).

[6] L. M. Wedepohl and D. J. Wilcox, "Estimation of transient sheath overvoltages in power-cable transmission systems", Proc. IEE, vol. 120, pp. 877-882, 1973.

[7] N. Nagaoka and A. Ametani, "A development of a generalized frequency-domain transient program – FTP", IEEE TPWRD, vol. 3, no. 4, pp. 1986-2004, 1988.

[8] A. Semlyen and A. Dabuleanu, "Fast and accurate switching transient calculations on transmission lines with ground return using recursive convolution", IEEE Trans. PAS, vol. 94, pp.561-571, 1975

[9] B. Gustavsen, J. Sletbak, and T. Henriksen, "Simulation of transient sheath overvoltages in the presence of proximity effects", IEEE TPWRD, vol. 10, no. 2, pp. 1066–1075, 1995.

[10] T. Noda, N. Nagaoka, and A. Ametani, "Phase domain modelling of frequency-dependent transmission lines by means of an ARMA model", IEEE TPWRD, vol. 11, no. 1, pp. 401–411, 1996

[11] A. Morched, B. Gustavsen, and M. Tartibi, "A universal model for accurate calculation of electromagnetic transients on overhead lines and underground cables", IEEE TPWRD, vol. 14, no. 3, pp. 1032–1038, 1999.

[12] T. C. Yu and J. R. Martí, "zCable model for frequency dependent modelling of cable transmission systems", IPST'2001, Rio de Janeiro, Brazil, Jun. 2001.

[13] U. S. Gudmundsdottir, "Modelling of long high voltage AC cables in transmission systems", Fredericia, Denmark: PhD. Thesis, Aalborg University, 2010, ISBN: 978-87-90707-73-6.

[14] N. Nagaoka and A. Ametani, "Transient calculations on crossbonded cables", IEEE Trans. PAS, vol. PAS-102, no. 4, pp. 779–787, 1983.

[15] U. S. Gudmundsdottir, B. Gustavsen, C. L. Bak, W. W. Wiechowski, "Field test and simulation of a 400-kV cross-bonded cable system", IEEE TPWRD, vol. 26, no. 3, pp. 1403-1410, 2011.

[16] A. Ametani, "Distributed-Parameter Circuit Theory". Tokyo: Corona Pub.Co., 1990.

[17] A. Ametani, N. Nagaoka, Y. Baba and T. Ohno, "Power system transients", New York, CRC Press, 2014.

[18] IEE Japan Working Group, "Surge phenomena and countermeasures on cable systems", IEE Japan Technical Report No.366, 1991.

[19] J. Mahseredjian, S. Dennetière, L. Dubé, B. Khodabakhchian and L. Gérin-Lajoie, "On a new approach for the simulation of transients in power systems", EPSR, Vol. 77, Issue 11, pp. 1514-1520, 2007.

[20] I. Koçar, J. Mahseredjian, G. Olivier, "Weighting method for transient analysis of underground cables", IEEE TPWRD, vol. 23, no. 3, 1629-1635, 2008.

[21] I. Koçar, J. Mahseredjian, G. Olivier, "Improvement of numerical stability for the computation of transients in lines and cables", IEEE TPWRD, vol. 25, no. 2, 1104-1111, 2010.

[22] H. W. Dommel, "EMTP theory book", Bonneville Power Administration, Portland, Oregon, 1986.

[23] A. Ametani (editor), "Numerical analysis of power systems transients and dynamics", IET, 2014. ISBN: 978-1-84919-849-3.

[24] B. Gustavsen, J. A. Martinez, and D. Durbak, "Parameter determination for modelling system transients—Part II: Insulated cables", IEEE TPWRD, vol. 20, no. 3, pp. 1045–2050, 2005.

[25] I. Lafaia, A. Ametani, J. Mahseredjian, A. Naud, M. T. Correia de Barros, I. Koçar, "Field test and simulation of transients on the RTE 225 kV cable", IEEE TPWRD (accepted for publication in Dec. 2015).

[26] A. Ametani, Y. Miyamoto, N. Nagaoka, "Semiconducting layer impedance and its effect on cable wave-propagation and transient characteristics", IEEE TPWRD, vol. 19, no. 4, pp. 1523-1531, 2004.

[27] I. Lafaia, N. Alatawneh, J. Mahseredjian, A. Ametani, M. T. Correia de Barros, I. Koçar, A. Naud, "Modeling of an underground cable installed in a poly-ethylene tube for transient simulations", IEEJ PES'2015, paper 5003, Aug. 2015, Nagoya, Japan.